Effects of the electrical parameters and gas flow rate on the generation of reactive species in liquids exposed to atmospheric pressure plasma jets

Eun Jeong Baek, Hea Min Joh, Sun Ja Kim, and T. H. Chung

Articles you may be interested in

Impact of plasma jet vacuum ultraviolet radiation on reactive oxygen species generation in bio-relevant liquids
Phys. Plasmas **22**, 122008 (2015); 10.1063/1.4934989

On the use of the double floating probe method to infer the difference between the electron and the heavy particles temperatures in an atmospheric pressure, vortex-stabilized nitrogen plasma jet
Rev. Sci. Instrum. **85**, 053507 (2014); 10.1063/1.4875215

Electrical characterization of the flowing afterglow of N2 and N2/O2 microwave plasmas at reduced pressure
J. Appl. Phys. **115**, 163303 (2014); 10.1063/1.4872468

Atmospheric-pressure plasma jets: Effect of gas flow, active species, and snake-like bullet propagation
Phys. Plasmas **20**, 023503 (2013); 10.1063/1.4791652

Electric probe investigations of microwave generated, atmospheric pressure, plasma jets
J. Appl. Phys. **108**, 013301 (2010); 10.1063/1.3448034

Effects of the electrical parameters and gas flow rate on the generation of reactive species in liquids exposed to atmospheric pressure plasma jets

Eun Jeong Baek, Hea Min Joh, Sun Ja Kim, and T. H. Chung[a)]
Department of Physics, Dong-A University, 604-714 South Korea

In this work, an atmospheric pressure plasma jet was fabricated and studied for plasma–liquid interactions. The plasma jet consists of a quartz-covered pin electrode and outer quartz tube with a tapered nozzle. Using the current–voltage (I-V) and optical emission characteristics of the plasma jet, the plasma density and the speed of the plume were investigated. The optical emission spectra clearly indicated the excited NO, O, OH, N_2, and N_2^+ in the plasma plumes. Then the plasma jets were applied to the deionized water. We investigated the effects of the operating parameters such as applied voltage, pulse frequency, and gas flow rate on the generation of reactive species in the gas and liquid phases. The densities of reactive species including OH radicals were obtained at the plasma–liquid surface and inside the plasma-treated liquids using ultraviolet absorption spectroscopy and chemical probe method. The nitrite concentration was detected by Griess assay. The data are very suggestive that there is a strong correlation among the production of reactive oxygen and nitrogen species (RONS) in the plasmas and liquids. *Published by AIP Publishing.*
[http://dx.doi.org/10.1063/1.4959174]

I. INTRODUCTION

Atmospheric pressure plasma jets (APPJs) can produce local non-thermal plasma, characterized by flexibility, compactness, and efficiency.[1–3] Since APPJs generate plasma plumes in open space surrounding air rather than in confined discharge gaps, they can be used for direct treatment and there are no limitations on the sizes of the objects to be treated. Research on the applications of APPJs has rapidly expanded to biology and medicine.[4–6] In particular, the use of APPJs in cancer therapies is drawing a great amount of attention because plasmas contain short lived free radicals, including reactive oxygen species (ROS), charged species, and electric fields, which can induce apoptosis in cancer cells. One of the most important factors is the plasma-generated reactive species including ROS. Over the past few years, a considerable number of studies have tried to increase the ROS in atmospheric pressure plasma medium for plasma bio/medical applications.

It has been known that when atmospheric pressure plasma jets are applied on the liquid containing cells, the plasma-induced reactive oxygen and nitrogen species (RONS) in the gas phase could generate long-living reactive species in the liquid which interact with cells resulting in intracellular RONS generation and apoptotic cell death.[4,5,7,8] In practice, diseased living tissues are either moist or covered by a layer of liquid. When a plasma jet is used to treat a living tissue, its plasma species are delivered to the air–liquid interface and then undergo transportation, and sometimes secondary RONS generation within the liquid medium, before reaching cells and tissues.

The cell culture media mediate the plasma effect on cell death and cell adhesion because of the interaction of plasma with organic components of cell culture media. Plasma generated from atmospheric air contains chemically reactive H, N, O, O_3, NO, NO_2, and OH radicals formed in large quantities. The final products of these unstable species in the liquid phase might be O_2 ($^1\Delta_g$), H_2O_2, O_3, NO_x, N_2O, and HNO_x, which are quite stable.[9,10] In the previous work, we observed that the richness of ROS in APPJ leads to better apoptotic rate.[7] Therefore, each plasma-generated agent that may have biological implication should be identified and quantitatively measured. These chemical species which include O, O_2^-, OH, NO, and NO_2 exhibit strong oxidative stress and/or trigger signaling pathways in biological cells. It is widely known that OH radicals are the building blocks of H_2O_2 which is considered as an important agent in the chemical reactivity of plasma in contact with liquids, and thus, OH plays an important role in plasma chemistry among others.[8]

In this work, plasma jets with a pin electrode are characterized to provide a plasma environment well suited for the treatment of thermally sensitive materials and biomedical materials. The effects of the electrical parameters (applied voltage and pulse frequency) and the gas flow rate on the discharge properties of plasma are investigated. The physical properties of the generated plume include the current–voltage characteristics, plume temperatures, and species compositions deduced from optical emission spectroscopy. Then, atmospheric pressure plasma jet was applied on the surface of liquid (deionized water). The reactive species including OH radicals generated in both the gas phase and the liquid phase (including the plasma–liquid surface) were measured using different diagnostic methods such as optical emission spectroscopy, ultraviolet absorption spectroscopy, and chemical probe method. Since the generation of reactive species

[a)]Author to whom correspondence should be addressed. Electronic mail: thchung@dau.ac.kr

23, 073515-1

strongly depends on the plasma control parameter, we investigate the effect of the operating parameters such as applied voltage, pulse repetition frequency, and gas flow rate on the reactive species generation at the gas–liquid interface and inside the liquid. Although plasma treatment of culture medium (here, deionized water) without cells is highly artificial, it may help us to understand the importance of the plasma effects in the liquid phase.

II. EXPERIMENTAL

An atmospheric pressure plasma jet was fabricated and characterized to provide a plasma environment well suited for living tissue treatment. The plasma jet consisted of a quartz confinement tube (outer quartz tube of tapered (funnel-shaped) cylinder) and a quartz-covered copper pin electrode. A schematic diagram is shown in Fig. 1. Both the outer quartz confinement tube (inner diameter $D = 10$ mm, length $L = 80$ mm) and the inner quartz tube served as the dielectric barrier layer. The jet had a central powered electrode (copper pin wire of diameter 1.0 mm).

A small diameter of the pin electrode with a sharp edge allowed for a local enhancement of the electric field and, thus, a considerable reduction of the breakdown voltage requirement. The helium plasma was generated by a pulsed bipolar source of up to 13 kV_{pp} with a repetition frequency of several tens of kilohertz (APP020 EESYS). A typical operation condition of the plasma jet had an applied voltage of 1.5 kV_{rms} (root-mean-square value), repetition frequency of 50 kHz, and pulse width of 5.5 μs. The waveforms of the voltage and the current were measured using a real time digital oscilloscope (LeCroy WS44XS-A) via high voltage probe (PPE 20 kV LeCroy) and current probe (Pearson 4100). The optical characteristics of the discharges were obtained by means of optical emission spectroscopy (USB-2000+XR-ES OceanOptics) to identify various excited plasma species produced from the plasma jet. In order to verify the general optical properties of the plasma jets, the optical emissions were also measured as a function of time. A photosensor amplifier (Hamamatsu C6386-01) was used to observe the wavelength-integrated plasma emission.

OH is one of the most active species generated in moist gas mixtures. Knowing the production mechanisms and measuring the absolute density of OH species will help the adjustment of treatment doses, and allow for optimization of the plasma process for a specific application.[11] OH radicals detected in the plasma-treated liquid are mainly originating in the gas phase, and not in the liquid (although a little OH generation is possible at the liquid interface by photo-dissociation of water molecules due to the UV originating from the plasma jet). The electron-impact reactions including those by plasma-activated neutral species play an important role in generating OH species in the gas phase. Thus, the plasma properties are deeply connected with the amount of RONS in plasma-treated liquid. In this study, we investigate the effect of the operating parameters such as applied voltage, repetition frequency, and gas flow rate of a pulsed bipolar APPJ on the generation of OH radicals at both the liquid surface and inside the liquid. Since the OH radicals in liquid contribute to cell death, a strong correlation between the production of OH in liquid phase and apoptosis rate of cancer cells is expected.

FIG. 1. Schematics of the experimental setup and the photographs of the plume. Diagnostics include current–voltage measurement, optical emission spectroscopy, ultraviolet absorption spectroscopy, and chemical probe method (TA was used as an OH radical trap).

To estimated OH radical density at the plasma–liquid surface, the plasma jet was applied on the liquid, and the spectra were obtained using ultraviolet (UV) absorption spectroscopy. The schematic experimental setup for the ultraviolet absorption spectroscopy at the liquid surface is presented in Fig. 1. This system consists of deuterium UV lamp, plano-convex lens, collimator lens, and a fiber optic spectrometer. The OH density can be calculated using Lambert–Beer's law.[12] The incident UV light on the liquid has the intensity (I_0) and the transmitted light intensity (I_ν). The light intensity has been absorbed by OH radical species during the passing through the distance x in the medium. The density of OH radicals from the plasma–liquid interaction is given by

$$N = -\frac{1}{\sigma \cdot x} \ln\left(\frac{I_\nu}{I_0}\right), \tag{1}$$

where N is the species of OH and σ is the cross sectional area of about 1.2×10^{-16} cm^2 for absorbing species of OH species in the gas phase.[12,13] Although σ is given in the gas phase, it could be used to give an estimate of OH radical density at the plasma–liquid interface.

UV absorption spectroscopy can be further used to estimate the long-living reactive species inside the plasma-treated liquid. The transmission spectra of the deionized water were recorded between 190 and 900 nm. These spectra were converted into absorbance (Abs) spectra using the equation[14,15]

$$Abs = -\ln\left(\frac{I_\nu}{I_0}\right). \tag{2}$$

RONS with relatively long estimated half-lives that are readily generated by atmospheric-plasmas contacting water include hydrogen peroxide (H_2O_2), nitrate (NO_3^-), nitrite (NO_2^-), and ozone (O_3).[14,15] These are expected to be the main species contributing to the UV absorbance signal. These RONS may be either primary RONS, generated directly by the plasma jet, or secondary RONS generated for example, at the surface of, or within, the medium.[14]

RONS in gas phase spread into liquid phase and react with water to produce various biologically active reactive species in the liquid phase. The presence of H_2O_2 accelerates the decomposition of ozone and increases the OH radical concentration in water.[16] As a method of OH radical detection, we utilized the hydroxylation of terephthalic acid (TA), which is a typical photocatalytic reaction that specifically oxidizes TA. That is, the OH radical reacts with TA to form hydroxyterephthalic acid (HTA) which fluoresces. When the solution containing TA and HTA molecules is irradiated by UV light, the HTA molecules emit light at $\lambda = 425$ nm, while the TA molecules do not.[8] Fluorescence intensity was observed to increase after reaction with plasma, indicating the total amount of OH radicals trapped by TA. The plasma was ignited and the liquid was exposed to the effluent. From the fluorescence intensity emitted from the post-exposure solution, the amount of OH radicals in plasma-treated liquids could be estimated.

Moreover, of special interest is the nitric oxide due to its crucial role in both cell death and proliferation.[17,18] There is a substantial literature on the role of NO and related compounds as a direct cancer therapy or as agent that re-sensitizes tumors to chemotherapy or radiation therapy.[19–21] These studies provide evidence of an important tumor apoptotic intercellular signaling mechanism involving NO and $ONOO^-$.[19–22] It appears that APP generates a chemistry (nitrite (NO_2^-), nitrate (NO_3^-) and peroxynitrite ($ONOO^-$)) that is closely related to the NO chemistry.[20,21] The NO is created as: $N_2 + e \rightarrow 2N + e$, $N + O + N_2 \rightarrow NO + N_2$, and $ONOO^-$ is produced by $NO + O_2 \rightarrow ONOO^-$. The majority of reactive nitrogen species (RNS) incident onto tissue are in the form of negative ions, dominantly, $ONOO^-$ and NO_3^-. RNS simply diffuses through the water layer.[23] In order to determine the NO levels delivered to growth media, the total nitrite concentrations are often measured. Nitrite concentration is determined using the Griess reagent (Molecular Probes®), which can spectrophotometrically detect nitrite formed by the spontaneous oxidation of NO under various conditions. Understanding the role of APP in generating NO_x^- containing species that may able to interact with complex biochemical processes will lead to extended applications in plasma cancer therapy.

III. RESULTS AND DISCUSSIONS

A. Electrical characteristics and plume generation

The temporal evolutions of the applied voltage, total and discharge current, and optical emission intensity are presented in Fig. 2 for the discharge operating at a frequency of 50 kHz. The current leads the voltage waveform, which indicates capacitive behavior of the dielectric barrier discharge. The voltage across the gas gap (V_g) is simply the difference between the applied voltage (V_a) and the voltage across the dielectric (V_d). Note that V_d follows temporally V_a with a time lag and the temporal profile of the total current resembles that of V_g as shown in Fig. 2(b). The time lag is due to the charges from the plasma volume being collected on the surface of the dielectric.[24] To determine the actual discharge current (Fig. 2(c)), the displacement current (I_{no}) with plasma off was subtracted from the total current (I_{tot}). For the gas flow rate of 1 l/min and the applied voltage of 1.58 kVrms (root-mean-square [rms] value), the total current typically reaches a peak value of 0.27 A (or rms value of 64 mArms). The rms value of the discharge current is about 3.2 mArms. The mean power transferred into the discharge is around 3.2 W.

Figures 2(d) and 2(e) represent the temporal evolutions of the wavelength-integrated optical emission intensities measured at the electrode end and nozzle end. It is observed that the discharge produced at least two plasma bullets every cycle of the applied voltage, that the main optical emission occurred at the rising period of the positive half cycle of the voltage waveform ("C"), and that the weak light emission signal occurred at the falling period of the negative half cycle ("A"). Another optical emission occurs at the rising period of the negative half cycle of the voltage waveform ("B"). But this peak due to the secondary discharge appears only near the electrode and does not propagate (see Fig. 2(e)). The main optical intensity measured at the electrode
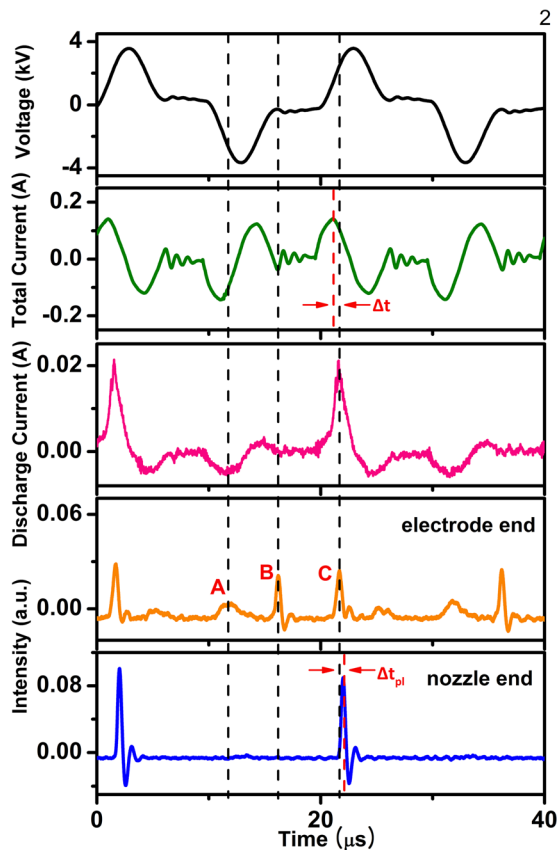
FIG. 2. Waveforms of (a) the applied voltages, (b) the total current, and (c) the discharge current for the jets driven by a pulsed bipolar source at 50 kHz. Temporal evolutions of the wavelength-integrated optical emission intensities at (d) the electrode end and (e) nozzle end. Here, the applied voltage (V_a) is 1.83 kVrms, and the gas flow rate (FR) is 1 l/min.

when the electrons move to the low field region. Therefore, the negative potential electrode tip is covered by an electron-cloud. These confined electron cloud produces weak light emission ("A").[25] However, a streamer discharge mechanism will be involved in the formation of the plasma plume when the applied voltage is very high. When the peak value of the applied voltage is high enough, these electrons generated at negative half cycle discharge will move toward the needle tip, and weak light emission can be discerned at the positive half cycle of the applied voltage.

Therefore, when the positive pulse is used, the local electric field induced by the plasma bullet and the electric field from the external applied voltage have the same direction, so the total electric field is enhanced, which results in the high peak velocity of the plasma bullet ("C"). On the other hand, when the negative pulse is used, the two electric fields mentioned above have opposite directions, so the total electric field is weakened, which is the reason why the peak velocity achieved by the positive pulse is higher than that resulting from the negative pulse ("A"), and there appears a weak negative current.[26] By the same reason, the optical emission at B does not contribute to the discharge current.

Figure 3 shows the change of the plasma plume current with different operating parameters (applied voltage, pulse frequency, and gas flow rate). The plume current–applied voltage curve reveals that the plasma jet exhibits abnormal glow regions where the discharge current increases monotonically with the applied voltage. When the applied voltage is in the range of 1.08–1.83 kVrms, the measured plume current is 0.38–0.95 mArms. The plume (discharge) current is observed to vary little with the variations of the pulse frequency and gas flow rate.

The plasma density is an important factor to examine the mechanism of plasma generation (thus, RONS production) in plasma jet.[27] The electron density may be estimated from plasma jet current measurements using the Ohm's law applied for the electron current.[28] The plasma electron density is obtained by the ratio between the discharge current density and the product of electron charge and drift velocity. The cross-section of plume was estimated from the observation of the plasma plume by photographs. It is known that a plasma bullet propagates due to the local electric field in front of the bullet head and the seed electrons which are either left from the previous discharge or are generated through photoionization.[29] The seed electrons move under the local electric field and result in avalanches, which contribute significantly to the discharge current. Thus, the

tip ("C") is found to be nearly in phase with the discharge current. However, the characteristics of light emission at the nozzle exit differ depending on the electrical parameters and gas flow rate, which may result from different drifting velocities of the charged species driven away from the electrode. The discharge current and the optical emission intensity indicate that stronger plasma bullets are generated in the positive half cycle of the voltage waveform.

The different optical intensity waveforms may result from different discharge mechanisms for corona mode ("A") and plasma plume mode ("C"). In the corona mode, electric field is strong in the vicinity of the needle tip, while it is weak elsewhere. Therefore, ionization and excitation processes can only occur in the strong field region. In the negative half cycle, the drifting velocity of electrons is very low
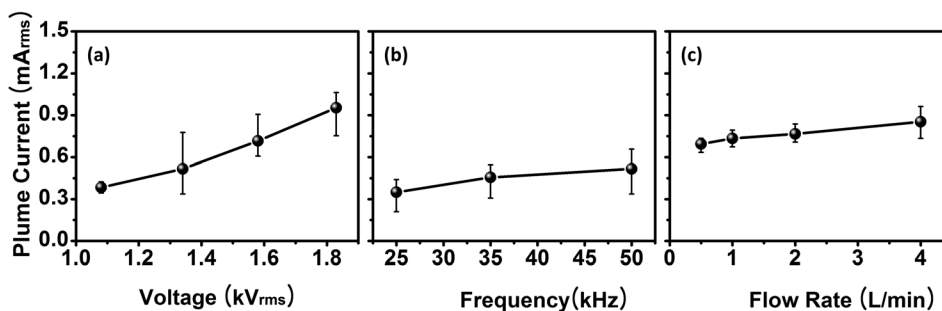

FIG. 3. Plume current as functions of (a) applied voltage (FR = 1 l/min), (b) pulse repetition frequency (V_a = 1.34 kVrms, FR = 1 l/min), and (c) gas flow rate (V_a = 1.58 kVrms).
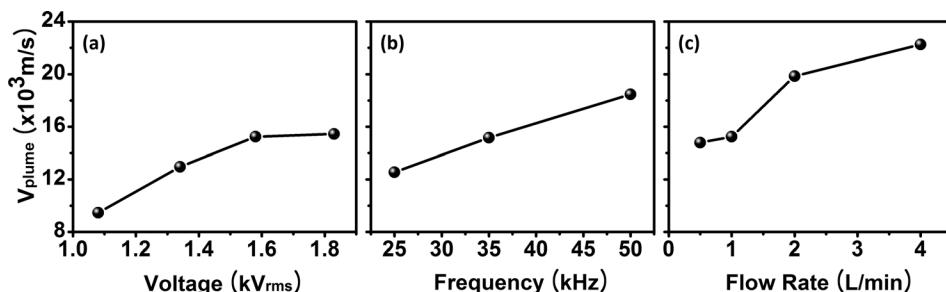
FIG. 4. Plume speed as functions of (a) applied voltage (FR = 1 l/min), (b) pulse repetition frequency (V_a = 1.58 kVrms), and (c) gas flow rate (V_a = 1.58 kVrms).
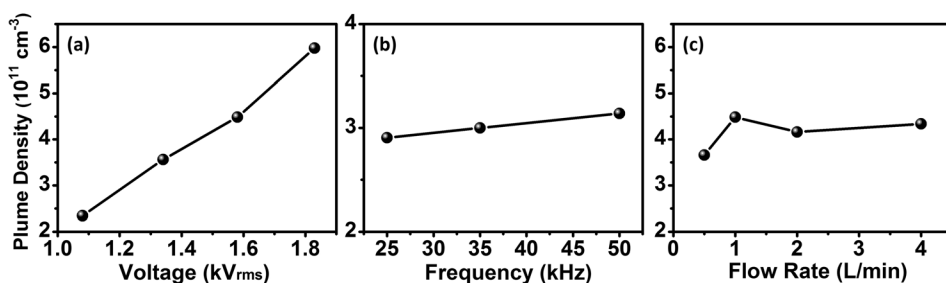

FIG. 5. Plume density as functions of (a) applied voltage (FR = 1 l/min), (b) pulse repetition frequency (V_a = 1.34 kVrms), and (c) gas flow rate (V_a = 1.58 kVrms).

electron drift velocity can be of the same order of magnitude as the propagation velocity of the plasma bullet.[30] As an approximation, we used the plasma bullets velocity as a maximum estimation of the drift velocity.[28–31] The traveling luminous bullet (corresponding to a positive streamer initiated by photoionization) can be detected by the plasma light emission at a specific position. The temporal delay (Δt_{pl}) between light emission signals from the two points with a fixed distance gives the propagation speed of the luminous bullet. It is observed in Fig. 4 that the drift velocity increases with increasing applied voltage, pulse frequency, and gas flow rate. With this information, we can estimate the changes of the plasma plume density with applied voltage, pulse frequency, and gas flow rate (Figs. 5(a)–5(c)). The plasma plume density is observed to increase with increasing applied voltage and pulse frequency. This is attributable to the fact that increasing applied voltage and pulse frequency results in faster, more intense ionization wave penetrating further into the plume. But, as the gas flow rate is increased, the plume density is observed to increase at first and then decrease at the flow rate greater than 1 l/min.

Figure 6 shows the measured plume temperature as functions of the applied voltage and gas flow rate. The plume temperature was measured using a fiber optic temperature sensor (Luxtron M601-DM&STF). As the applied voltage was increased, a continuous increase in the plume temperature

was observed (Fig. 6(a)). An increase in the applied voltage leads to an increase of the plasma volume, which is immediately reflected by gas heating. The plume temperature depends on the plume current and on the gas flow characteristics. The plume temperature is observed to decrease as the gas flow rate is increased (Fig. 6(b)). This seems to be mainly attributed to a rise in collision frequency of hot plasma species with the surrounding cold molecules, effectively leading to a reduction in the plume temperature.[32] These results indicate that the plume temperature can be adjusted effectively by controlling the gas flow rate.[33]

B. Optical characteristics

To identify reactive species that are generated in the discharge and subsequently expelled with the gas flow, optical emission spectra were recorded in the wavelength range from 200 nm to 900 nm (Fig. 7(a)). The spectrum shows that there are strong nitrogen molecular lines as well as a few helium and oxygen atomic lines. Oxygen and nitrogen species arise because the plasma is ejected into the air where its energetic electrons and He metastables ionize and excite air molecules. The strongest emission was the N_2^* line at 337.1 nm ($C^3 \Pi_u \rightarrow B^3 \Pi_g$), and many nitrogen lines, excited He atom line at 706.5 nm, and excited oxygen line at 777.4 nm are shown. The N_2^+ line at 391 nm ($B^2\sum_u^+ \rightarrow X^2\sum_g^+$) is attributed to
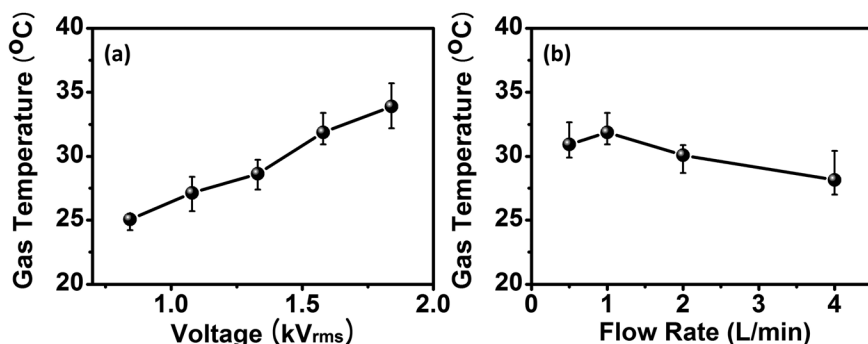

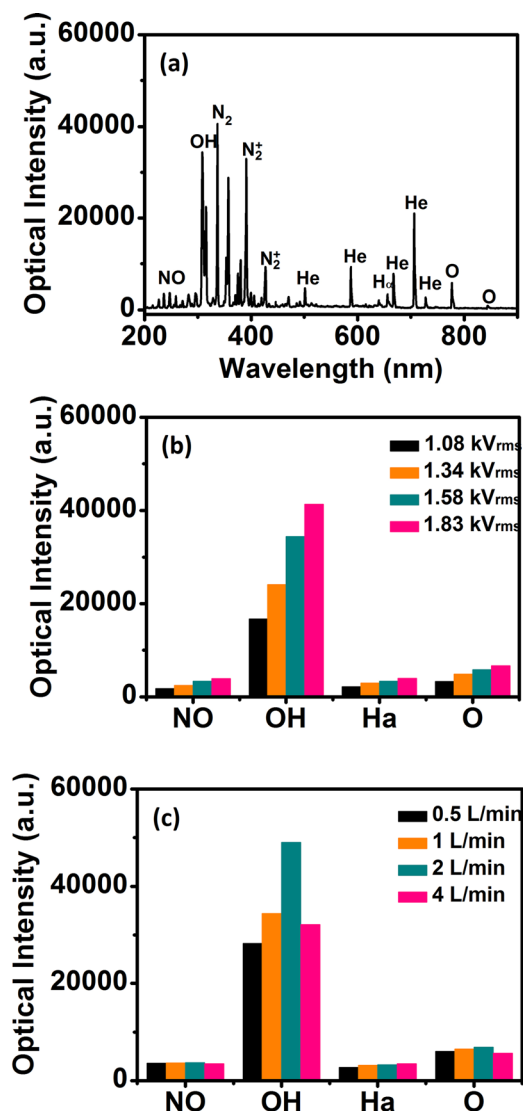FIG. 6. Plume temperature as functions of (a) applied voltage (FR = 1 l/min) and (b) gas flow rate (V_a = 1.58 kVrms).

FIG. 7. (a) Emission spectra from 200 nm to 900 nm observed in the He jet ($V_a = 1.58$ kVrms, FR = 1 l/min). Variations of the emission intensities from NO, OH, H, and O as functions of (b) applied voltage and (c) gas flow rate.

such as O, OH, and NO are considered to be the most effective agents in attacking cells or organic material in general.

Figures 7(b) and 7(c) show the variations of the emission intensities of NO, OH, O, and H_α via the optical spectra with the applied voltage and gas flow rate, respectively. It should be noted that the emission intensity depends on the densities of the excited species and the surrounding electrons, the quenching rate, the emission characteristics (light frequency, spontaneous emission probability, and branching ratio), and the spectral response of the detection system. Therefore, it is difficult to infer the variation of species densities from the emission intensities. However, a given emission intensity from a species can be regarded as a measure of the concentration of the species for a qualitative analysis. It is observed that operation conditions under higher applied voltage result in the richness of these reactive species. Significant effect of increasing voltage is that the faster, more intense ionization wave penetrates further into the plume, and this creates more reactive species. The effect of gas flow rate is more complicated. As the gas flow rate is increased, the line intensities of O, H_α, OH, and NO increase, reaching the maximum at 2 l/min, and then decrease. On the other hand, the intensity of N_2^+ band decreases with increasing gas flow rate. The decrease in N_2^+ can be explained by several factors: the reduction of Penning ionization of N_2^+ due to the reduced inclusion of N_2 or the reduction of the electron impact excitation. The decrease in OH concentration at 4 l/min can be explained by the fact that the jet elongation caused by an increase in gas flow rate led to a decrease in power density.[36] Since the electron-impact dissociation of H_2O appears to be the most important reaction to produce OH species, the evolution of the electron density with the flow rate should be taken account. It is also observed that as the pulse frequency is increased, the emission intensity of all the peaks increase slightly (not shown).

C. OH density at the plasma–liquid interface

Figure 8(a) shows the UV absorption spectral profile caused by the OH species at the plasma–liquid interface. Using Eq. (1), the OH density at the liquid surface is measured as functions of the applied voltage, pulse frequency, and gas flow rate (Figs. 8(b)–8(d)). As expected from the discussion of the plume density (Figs. 5(a) and 5(b)), the OH density is observed to increase with increasing applied voltage and pulse frequency.

The gas flow affects the OH concentration in different ways.[36] On one hand, the gas flow has a significant effect on the air diffusion into the working gas stream. The higher is the flow rate, the longer is the He gas stream with the low air fraction. This explains the elongation of the jet with increasing flow rate. On the other hand, plasma generation can also strongly influence the gas flow at the jet outlet,[37] and when the gas flow is increased to certain level (in this study, 4 l/min), the gas flow changes from the laminar to the turbulent mode and the length of the He gas stream with the low air fraction decreases significantly. The results show that the OH density first increases with increasing gas flow rate from 0.5 to 2 l/min. At around 2.0 l/min, it is found that the density
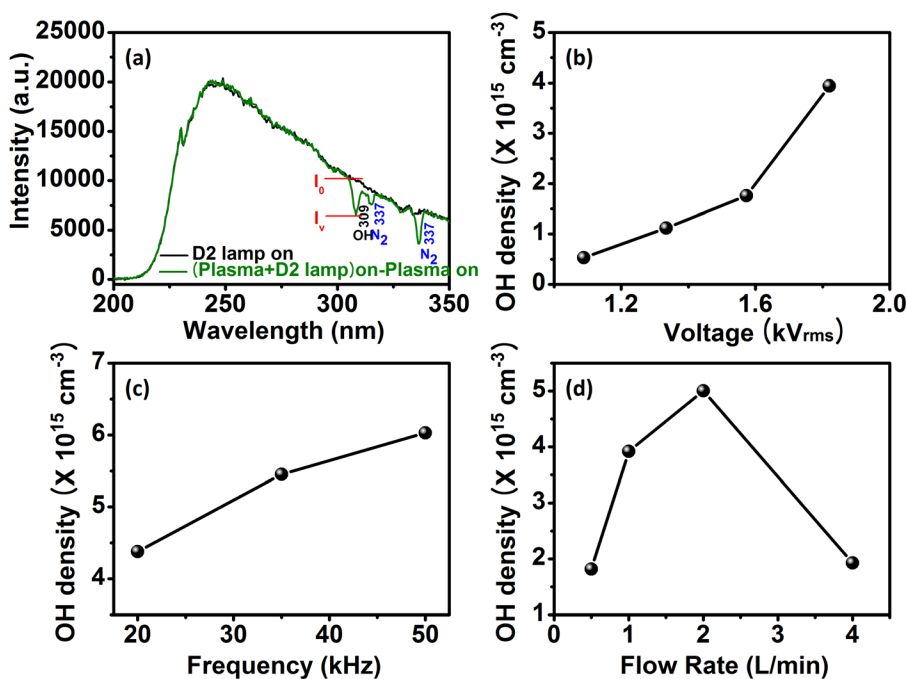
Penning ionization ($He^* + N_2 \rightarrow He + N_2^+ + e^-$) and charge transfer ($He^+ + N_2 \rightarrow He + N_2^+$) followed by direct electron-impact excitation ($e^- + N_2^+ \rightarrow N_2^{+*} + e^-$).[34] In the discharge area, the electron impact dissociation of N_2 and O_2 molecules leads to the formation of atomic oxygen and the breaking of the strong bond in the N_2 molecule by vibrational excitation and dissociation. Atomic oxygen may also be generated though Penning dissociation ($N_2^* + O_2 \rightarrow N_2 + O + O$) and ($He^* + O_2 \rightarrow He + O^* + O$). The emission line at 656 nm corresponds to the H_α line, which is generated by the collision between water vapor molecule and electrons ($H_2O + e \rightarrow H + OH + e$). The emission spectrum clearly indicates that OH (309 nm) and NO (283 nm) exist in the plasma plume. The OH radicals are produced from water vapor in the helium flow, which is humidified by water adsorbed on the inner surface of the helium line and the quartz tube.[35] The presence of nitric oxide (NO) at 283 nm is due to the chemical conversion of N and O_2 (or N and O). The NO serves a multitude of essential biological functions. These highly reactive species

FIG. 8. (a) UV absorption spectral profile caused by the OH species at the plasma–liquid interface ($V_a = 1.58$ kVrms, FR = 1 l/min). Estimated OH density as functions of (b) applied voltage, (c) pulse frequency, and (d) gas flow rate. In (c) and (d), $V_a = 1.58$ kVrms.

of hydroxyl OH radical species reaches the maximum value of 5×10^{15} cm^{-3}. It is also noted that the OH density rapidly decreases to 2×10^{15} cm^{-3} as the gas flow rate is increased to 4 l/min.

D. OH density in the liquid phase

Figure 9 shows the fluorescence spectra of HTA as functions of applied voltage and gas flow rate. Aqueous solution of TA was prepared by dissolving TA (Sigma) in distilled water containing NaOH (Wako). The initial concentrations of
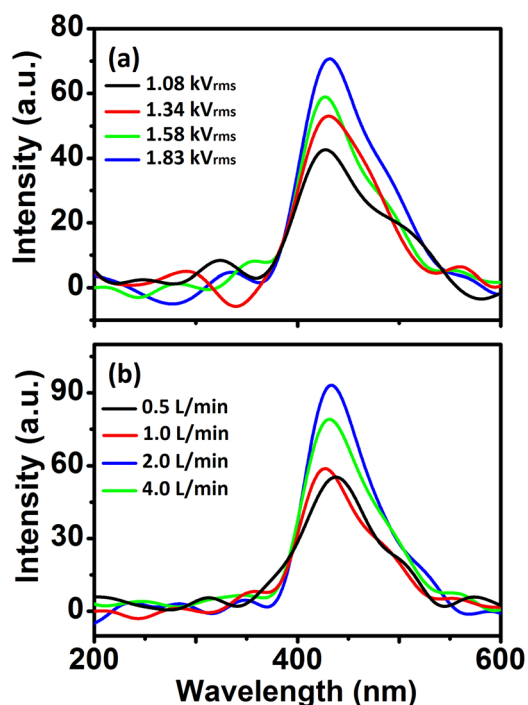
FIG. 9. Fluorescence spectra of aqueous TA solutions exposed to the APPJ. The dependence on (a) applied voltage (FR = 1 l/min), (b) pulse frequency ($V_a = 1.58$ kVrms, FR = 1 l/min), and (c) gas flow rate ($V_a = 1.58$ kVrms).

TA and NaOH were 3 mM and 10 mM, and the initial value of pH was 8. The dish plate (diameter 20 mm) including liquids was irradiated with plasma (for 5 min), and samples of the liquids from dish after plasma treatment were taken using a cuvette to observe the fluorescence after exciting by light source. In our previous experiment[38] utilizing different jet devices and power sources, as the applied voltage and pulse repetition frequency were increased, the fluorescence intensity increased, indicating an increase in the total amount of OH radicals trapped by TA. In this work, the OH density increases with the applied voltage as shown in Fig. 9(a), in agreement with the previous measurement of the OH density.[8,39] These observations are in a similar trend to those of the intensity level of OH in optical spectra (Fig. 7(b)).

Concerning the gas flow rate dependence, the gas flow rate of 2 l/min has the highest fluorescence followed by 4, 1, and 0.5 l/min (Fig. 9(b)). This indicates that adequate gas flow promotes the transport of RONS into liquid.[14] High flow rate results in short residence times and RONS flowing out of the tube increase.[40] However, at the flow rate of 4 l/min, we observe a decrease in the production of reactive species. This can be explained by the similar effects discussed in Section III C. These data also indicate that the increase of OH radicals in the liquid phase results from the plasma–liquid interaction (Fig. 8(d)). These observations are not in contradiction with the change of the emission intensity level of OH (Fig. 7(c)). Therefore, we can expect a decrease in the overall inventory of OH in liquid at higher flow rate (above 4 l/min).

E. UV absorbance

The UV absorbance is a measure of the long-living reactive species present in the plasma-treated liquid. As shown in Fig. 10(a), the UV absorbance increases with increasing applied voltage. The growth of applied voltage leads to an increase of the densities of all the reactive species. Concerning
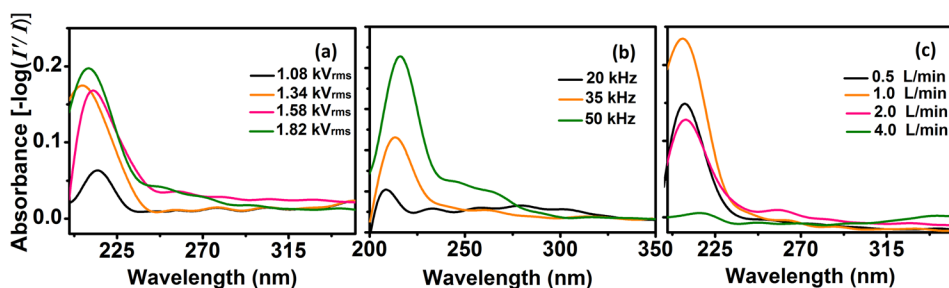
FIG. 10. UV absorption measurements of the deionized water exposed to the APPJ with varying (a) applied voltage (FR = 1 l/min), (b) pulse frequency (V_a = 1.34 kVrms, FR = 1 l/min), and (c) gas flow rate (V_a = 1.58 kVrms).
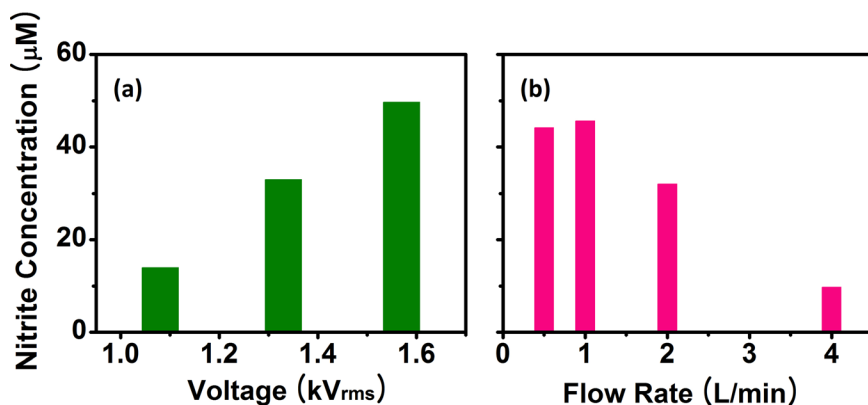

FIG. 11. Measurement of nitrite concentration with increasing (a) applied voltage (FR = 1 l/min) and (b) gas flow rate (V_a = 1.58 kVrms) in deionized water after plasma treatment.

the gas flow rate dependence, the gas flow rate of 1 l/min has the highest absorbance followed by 0.5, 2, and 4 l/min (Fig. 10(b)). This indicates that the case of 1 l/min produces more accumulation of H_2O_2, NO_3^-, NO_2^-, and O_3. This result agrees overall with the OH emission in the gas phase (Fig. 7(c)) and the change in the OH density at the plasma–liquid interface and inside the liquid with varying gas flow rates (Figs. 8(d) and 9(b)). This observation is attributable to the effects of the plasma density (Fig. 5(c)) of the plume contacting liquids, which generates the reactive species.

F. Measurement of nitrite concentration

Figure 11 shows the measurement of nitrite concentration with increasing applied voltage and gas flow rate in deionized water after plasma treatment by Griess assay. NO_2^- and NO_3^- are the metabolic products of NO and are convenient markers of NO formation. The detected nitrite concentration became higher with increasing applied voltage. Because the generation mechanism of NO has a lot of routes closely connected to that of OH,[41] the nitrite concentration has a similar dependence on operating parameters to the OH concentration. The result also shows that the highest nitrite concentration occurs at the gas flow rate of 1 l/min, which is consistent with the result of UV absorbance (Fig. 10(b)) exhibiting the accumulation of H_2O_2, NO_3^-, NO_2^-, and O_3.

Our previous studies[7,42] indicated that apoptosis in plasma-treated cancer cells in-vitro increased with increasing applied voltage and pulse repetition frequency, and that the volume and luminosity of plasma bullet increased in the same manner. These observations well agree with the dependence of RONS (measured in gas and liquid phases) on applied voltage and pulse frequency.

IV. CONCLUSIONS

Atmospheric pressure helium plasma jets excited by a low-frequency pulsed bipolar source were fabricated and characterized. The electrical characteristics of the jet, the plume length, and the ability to produce reactive species exhibited quite a strong dependence on the electrical parameters and gas flow rate. The consequences of applied voltage, pulse repetition frequency, and gas flow rate on RONS production were investigated. The OH density was measured at the liquid phase by UV absorption spectroscopy and compared with the OH density in the gas phase measured by optical emission spectroscopy. The OH concentration in the liquid was also measured by a chemical probe method using TA solution. The changes in the OH density in the gas phase with varying operating parameters exhibited similar trends to those of the concentrations OH and the long-living reactive species in the plasma-treated liquids. The results are very suggestive that there is a strong correlation among the production of RONS in the plasmas and liquids. The applied voltage has the greatest influence on the production of RONS. The increases in applied voltage and pulse frequency led to the increases in the densities of OH and NO in the gas and liquid phase. The OH concentration increased with the gas flow rate in the range of 0.5–2 l/min and decreased at the flow rate greater than 2 l/min. Under the conditions of present experiments, it can be concluded that the application of high voltage with 50 kHz frequency and gas flow rate of 1–2 l/min results in the efficient production of reactive species. Since the various discharge parameters and ambient gas can influence the amount of OH radicals that can cause different plasma-induced chemistry effects, further experimental investigations are needed to consider the effects of variable plasma properties.

ACKNOWLEDGMENTS

[1]M. Laroussi and T. Akan, Plasma Processes Polym. **4**, 777 (2007).

[2]J. L. Walsh, F. Iza, N. B. Janson, V. J. Law, and M. G. Kong, J. Phys. D: Appl. Phys. **43**, 075201 (2010).

[3]J. L. Walsh and M. G. Kong, Appl. Phys. Lett. **93**, 111501 (2008).

[4]M. Keidar, A. Shashurin, O. Volotskova, M. A. Stepp, P. Srinivasan, A. Sandler, and B. Trink, Phys. Plasmas **20**, 057101 (2013).

[5]M. Vandamme, E. Robert, S. Lerondel, V. Sarron, D. Ries, S. Dozias, J. Sobilo, D. Gosset, C. Kieda, B. Legrain, J.-M. Pouvesle, and A. L. Pape, Int. J. Cancer **130**, 2185 (2012).

[6]X. Yan, Z. Xiong, F. Zou, S. Zhao, X. Lu, G. Yang, G. He, and K. Ostrikov, Plasma Processes Polym. **9**, 59 (2012).

[7]H. M. Joh, S. J. Kim, T. H. Chung, and S. H. Leem, Appl. Phys. Lett. **101**, 053703 (2012).

[8]K. Ninomiya, T. Ishijima, M. Imamura, T. Yamahara, H. Enomoto, K. Takahashi, Y. Tanaka, Y. Uesugi, and N. Shimizu, J. Phys. D: Appl. Phys. **46**, 425401 (2013).

[9]K. Panngom, K. Y. Baik, M. K. Nam, J. H. Han, H. Rhim, and E. H. Choi, Cell Death Dis. **4**, e642 (2013).

[10]W. Van Gaens and A. Bogaerts, J. Phys. D: Appl. Phys. **46**, 275201 (2013).

[11]X. Y. Liu, X. K. Pei, K. Ostrikov, X. P. Lu, and D. W. Liu, Phys. Plasmas **21**, 093513 (2014).

[12]H. P. Dorn, R. Neuroth, and A. Hofzumahaus, J. Geophys. Res. **100**, 7397, doi:10.1029/94JD03323 (1995).

[13]Y. H. Kim, Y. J. Hong, K. Y. Baik, G. C. Kwon, J. J. Choi, G. S. Cho, H. S. Uhm, D. Y. Kim, and E. H. Choi, Plasma Chem. Plasma Process **34**, 457 (2014).

[14]E. J. Szili, J.-S. Oh, S.-H. Hong, A. Hatta, and R. D. Short, J. Phys. D: Appl. Phys. **48**, 202001 (2015).

[15]S. Baldus, D. Schröder, N. Bibinov, V. Schulz-von der Gathen, and P. Awakowicz, J. Phys. D: Appl. Phys. **48**, 275203 (2015).

[16]P. Lukes, E. Dolezalova, I. Sisrova, and M. Clupek, Plasma Sources Sci. Technol. **23**, 015019 (2014).

[17]X. Han, M. Klas, Y. Liu, M. S. Stack, and S. Ptasinska, Appl. Phys. Lett. **102**, 233703 (2013).

[18]A. R. Gibson, H. O. McCarthy, A. A. Ali, D. O'Connell, and W. G. Graham, Plasma Processes Polym. **11**, 1142 (2014).

[19]D. B. Graves, Plasma Processes Polym. **11**, 1120 (2014).

[20]D. Hirst and T. Robson, J. Pharm. Pharmacol. **59**, 3 (2007).

[21]D. G. Hirst and T. Robson, Curr. Pharm. Des. **16**, 45 (2010).

[22]G. Bauer, Anticancer Res. **34**, 1467 (2014).

[23]W. Tian and M. J. Kushner, J. Phys. D: Appl. Phys. **47**, 165201 (2014).

[24]M. Laroussi, X. Lu, V. Kolobov, and R. Arslanbekov, J. Appl. Phys. **96**, 3028 (2004).

[25]X. Li, N. Yuan, P. Jia, and J. Chen, Phys. Plasmas **17**, 093504 (2010).

[26]Z. Xiong, X. Lu, Y. Xian, Z. Jiang, and Y. Pan, J. Appl. Phys. **108**, 103303 (2010).

[27]K. Yambe, S. Taka, and K. Ogura, Phys. Plasmas **21**, 043511 (2014).

[28]A. V. Nastuta, V. Pohoata, and I. Topala, J. Appl. Phys. **113**, 183302 (2013).

[29]G. Naidis, J. Phys. D: Appl. Phys. **44**, 215203 (2011).

[30]J. Gou, Y. Xian, and X. Lu, Phys. Plasmas **23**, 053508 (2016).

[31]E. Karakas, M. A. Akman, and M. Laroussi, Plasma Sources Sci. Technol. **21**, 034016 (2012).

[32]M. Klas and S. Ptasinska, Plasma Sources Sci. Technol. **22**, 025013 (2013).

[33]T. L. Ni, F. Ding, X. D. Zhu, X. H. Wen, and H. Y. Zhou, Appl. Phys. Lett. **92**, 241503 (2008).

[34]W.-C. Zhu, Q. Li, X.-M. Zhu, and Y.-K. Pu, J. Phys. D: Appl. Phys. **42**, 202002 (2009).

[35]S. Yonemori, Y. Nakagawa, R. Ono, and T. Oda, J. Phys. D: Appl. Phys. **45**, 225202 (2012).

[36]X. Lu, G. V. Naidis, M. Laroussi, S. Reuter, D. Graves, and K. Ostrikov, Phys. Rep. **630**, 1 (2016).

[37]X. Pei, M. Ghasemi, H. Xu, Q. Hasnain, S. Wu, Y. Tu, and X. Lu, Plasma Sources Sci. Technol. **25**, 035013 (2016).

[38]S. J. Kim and T. H. Chung, Appl. Phys. Lett. **107**, 063702 (2015).

[39]X. Pei, S. Wu, Y. Xian, X. Lu, and Y. Pan, IEEE Trans. Plasma Sci. **42**, 1206 (2014).

[40]S. A. Norberg, E. Johnsen, and M. J. Kushner, Plasma Sources Sci. Technol. **24**, 035026 (2015).

[41]A. Komuro, R. Ono, and T. Oda, J. Phys. D: Appl. Phys. **46**, 175206 (2013).

[42]S. J. Kim and T. H. Chung, IEEE Trans. Plasma Sci. **39**, 2280 (2011).